Article

Not peer-reviewed version

Spray Parameters and Coating Microstructure Relationship Study in Suspension Plasma Spray TiO2 Coatings

Garima Mittal , Nigar Gul Malik , Arunima Bhuvanendran Nair Jayakumari , David F Martelo , Namrata Kale , Shiladitya Paul *

Posted Date: 25 October 2023

doi: 10.20944/preprints202310.1545.v1

Keywords: suspension plasma spray; TiO2 coatings; coating microstructures; spray parameters

Article

Spray Parameters and Coating Microstructure Relationship Study in Suspension Plasma Spray TiO_2 Coatings

Garima Mittal [1], Nigar Gul Malik [1], Arunima Bhuvanendran Nair Jayakumari [1], David Martelo [2], Namrata Kale [2] and Shiladitya Paul [1,2,*]

[1] Materials Innovation Centre, School of Engineering, University of Leicester, Leicester, UK; garima.nano@gmail.com (Garima Mittal); ngm11@leicester.ac.uk (Nigar Malik); abnj1@leicester.ac.uk (Arunima Bhuvanendran Nair Jayakumari)

[2] Materials Performance and Integrity Group, TWI, Cambridge, UK; shiladitya.paul@twi.co.uk (Shiladitya Paul); david.martelo@twi.co.uk (David Martelo); namrata.kale@twi.co.uk (Namrata Kale)

* Correspondence: shiladitya.paul@twi.co.uk;

Abstract: In recent years, there has been growing interest in thermal spray techniques using suspension or solution-based coatings. These techniques offer precise control over particle size and microstructure, improving feedstock flowability and allowing for high-quality coatings customization. Spray parameters, such as stand-off distance (SOD) and feedstock flow rate, can alter the performance and characteristics of these coatings. Geothermal power plant heat exchangers often face issues like corrosion, scaling, and fouling. These issues could be mitigated, at least in part, by the use of spray coatings. In this study, TiO_2 coatings were applied to a carbon steel substrate using suspension plasma spray (SPS) to enhance the performance of geothermal heat exchanger materials. The impact of SOD (50, 75, and 100mm) and feedstock flow rate (10, 20, and 30 ml/min) on these coatings was examined through various techniques, including SEM, profilometry, XRD, and adhesion testing. The results demonstrated that coatings deposited using 10ml/min feedstock flow rate were well-adhered to the substrate due to efficient melting of coating material but as the SOD and feedstock flow rate increase due to poor thermal and kinetic energy exchange between the torch and feedstock particles, adhesion between coating and substrate decreases.

Keywords: suspension plasma spray; TiO_2 coatings; coating microstructures; spray parameters

1. Introduction

Geothermal energy is a potential source of sustainable and renewable energy. However, despite having the ability to provide clean and reliable power generation, geothermal energy has yet to reach its full potential. Because the performance and durability of various components of geothermal power plants are under constant threat of corrosion and scaling due to harsh environmental conditions such as high temperature, varied pH, humidity, silica, and acids [1], these issues adversely affect the stability and efficiency of the power plant, leading to increased operation and maintenance (O&M) costs. Stainless steel and titanium are the most commonly used materials that are used in designing geothermal plants' components. Stainless steel provides corrosion resistance, high-temperature sustainability, excellent mechanical strength, and durability. Titanium is also an excellent choice for geothermal heat exchangers due to its lightweight and outstanding corrosion resistance. Material selection depends on the geothermal fluid chemistry influenced by geographical location and heat exchanger configuration. In the long term, replacing components of the heat exchanger is expensive as compared to applying paints and coatings on the geothermal plant's components. Coatings designed for geothermal power plant components, particularly geothermal heat exchangers, could be a feasible and economical solution, providing protection against extreme thermal gradients, aggressive fluids, and mechanical stress.. Furthermore, coatings, especially micro/nanostructured surfaces play a crucial role in improving the overall efficiency and reliability of geothermal energy generation [2].

 doi:10.20944/preprints202310.1545.v1

Thermal spray coatings have gained attention due to depositing high-quality coatings with tailored properties. Conventional powder-based thermal spray is widely accepted and employed in various industries but when it comes to depositing very small particles (<10 microns), poor injection due to low inertia of particles restricts the use of gas as a carrier . Therefore, liquid carrying submicron particles (suspension) or a solution of chemical precursors of the coating material, forming solid particles during flight are preferred so that coatings with nano- and micro-scale features can be obtained.[3]. Besides, using liquid in the form of suspension or solution or both provides better flowability of the feedstock as well as enhanced control over coating microstructures [4]. There is no specific microstructure that is suitable for each geothermal heat exchanger as the choice of microstructure is influenced by different factors including geothermal plant location (as the geothermal fluid chemistry and constituents vary with the location of the geothermal plant) and types of heat transfer (boilers, condensers, and evaporators). Geothermal heat exchangers' components are exposed to high temperature and pressure, harsh chemicals and mechanical stresses. Therefore, microstructure of thermal spray coating needs to be engineered to resolve these issues, accordingly. For example, coatings with columnar microstructures are suitable for facilitating thermal cycling resistance but simultaneously, they might not be suitable for providing proper protection against corrosive environment due to the ingress of corrosive agents into the substrate. Similarly, coatings with vertically cracked microstructures could allow stress relief, decreasing the risk of coating delamination. But simultaneously, excessive cracking might compromise the structural integrity of the coating. Generally, dense coatings with controlled cracking or columnar structures are preferred in geothermal environment, providing better protection against corrosive agents along with the tolerance for thermal cycling. For better control over coating microstructure and properties, it is essential to understand the relationship between coating deposition/spray parameters and coating properties. The performance and characteristics of liquid feedstock-based thermal spray coatings are influenced by numerous key depositing parameters, for instance, feedstock type, feedstock flow rate, particle size, feedstock concentration, solvent type, plasma current and voltage, primary gases' type and flow rate, stand-off distance, and substrate size, shape, and temperature [5].

In this study, suspension plasma spray (SPS) was used to deposit TiO_2 coatings onto a carbon steel substrate. TiO2 coatings were chosen to protect the geothermal heat exchangers' components against corrosion and erosion as geothermal fluids contain abrasive particles, and to provide high-temperature stability and chemical stability to geothermal heat exchanger components protecting them against extreme heat conditions. Besides there are many reports available mentioning that the use of TiO2 coatings in heat exchangers improving their thermal conductivity [6]. These coatings are formed using an aqueous suspension of TiO_2 nanoparticles as the feedstock material. The aqueous suspension was chosen due to cost-effectiveness, environmental considerations, safety concerns and avoiding waste disposal issues. The effect of standoff distance (SOD; the distance between the injector nozzle and substrate surface) and feedstock flow rate (the rate at which the suspension feedstock is delivered to the spray gun) on coating microstructure was focused that is crucial for optimizing the coating process and attaining desirable coating performance. The SOD and feedstock flow rate influence the critical parameters of coating deposition, such as particle velocity, heat transfer, cooling rate, and adhesion. As soon as suspension feedstock is introduced into the system, it fragments into droplets due to having contact with the plasma plume, followed by solvent evaporation and coating material agglomeration because of high-enthalpy sintering and melting. Due to the acceleration toward the substrate, these feedstock droplets hit the substrate and form splats, developing coating through continuous stacking of splats [7].

Comprehensive analyses of coatings deposited via systematically varied SOD, and the feedstock flow rate was done using scanning electron microscopy (SEM), roughness measurements, and tape adhesion test. The findings of this work will help in optimizing the SPS of TiO_2 coatings on geothermal heat exchangers, enhancing their corrosion resistance, scaling resistance, and fouling resistance.

2. Materials and Methods

Preprints (www.preprints.org) | NOT PEER-REVIEWED | Posted: 25 October 2023 doi:10.20944/preprints202310.1545.v1

2.1. Substrate material

Coatings were developed on 25x25x6mm coupons of carbon steel (S275JR, EN 10025-2). Prior to coating deposition, carbon steel substrates were grit-blasted with #100 mesh white alumina to improve coating adhesion. Grit blasting parameters were 80 psi set pressure (70 psi run pressure) at 80 mm SOD. This process was followed by degreasing with acetone to clean the samples just before the coating deposition. The average surface roughness (R_a) of the substrate after grit blasting was 2.32µm.

2.2. Coating material

Aqueous suspension of 5 wt.% TiO_2 nanoparticles, commercially obtained from Promethean Particles Ltd., UK, were used as feedstock material. Since the feedstock was a homogeneous suspension of nanoparticles, no pretreatment was required. The particle size of TiO_2 in the suspension was 5-10nm as characterized by the supplier.

2.3. Coating development

Suspension plasma spraying was performed using a Praxair®®SG-100 plasma gun attached to an OTC AII-V20 robot. The APS plasma console was 3710 with HF 2210 starter kit. The horizontal speed of the robot was 450 mm/sec with a 5mm vertical increase. The suspensions were fed radially into the plasma through a syringe pump (ISCO®® 260D) connected to the external nebulizer (constructed from a modified RS air brush AB931). The diameter of the injector was 0.5mm. Suspension plasma spraying (SPS) was performed at a plasma current of 700 A and voltage of 46 V. A combination of argon (49 L/min) and hydrogen (0.9 L/min) gases was used as a plasma source, and argon (3 L/min) was used as a carrier gas. The number of passes was kept constant, i.e., 50, during plasma trials. The summary of plasma spray is given in Table 1:

Table 1. Summary of suspension plasma spray parameters.

Sample name	Feedstock flow rate	Standoff distance
Ti-50-10	10 mL/min	50 mm
Ti-50-20	20 mL/min	50 mm
Ti-50-30	30 mL/min	50 mm
Ti-75-10	10 mL/min	75 mm
Ti-75-20	20 mL/min	75 mm
Ti-75-30	30 mL/min	75 mm
Ti-100-10	10 mL/min	100 mm
Ti-100-20	20 mL/min	100 mm
Ti-100-30	30 mL/min	100 mm

2.4. Coating characterisation

The coating mass was determined by measuring the difference in weight between the sample after and before coating application. A Sartorius CPA324S four-figure Analytical Balance was employed for this weighing process. Deposition efficiency (DE), which indicates the productivity of the process for different spray conditions, was calculated based on ISO 17836:2017 [8] using the following formula (eqn. (1)):

$$DE\ (\%) = \frac{\text{Mass difference of the test piece}}{\text{Mass of spray material fed through}} * 100 \quad (1)$$

An EVO LS15 SEM (Zeiss) was used to characterise the top-view morphology and the cross-section of the coated samples. An acceleration voltage of 20 kV was used at a working distance of 8.5 mm. For cross-sectional SEM imaging, cross-sections were cut using a slow-speed precision saw and mounted in cold EpoFix resin (Buehler), followed by grinding (SiC papers P120, P320, P600, P1200, and P2500) and polishing (with 3µm and 1 µm clothes). XRD analysis was performed to assess the phase composition of suspension plasma spray TiO_2 coatings, using a Bruker AXS D8 diffractometer

Preprints (www.preprints.org) | NOT PEER-REVIEWED | Posted: 25 October 2023 doi:10.20944/preprints202310.1545.v1

with Cu Kα radiation source with λ 0.1542nm at 40KV and 100mA. Scans were taken from 10° to 90° 2θ range with 0.02 steps per second scan rate. The volume percentage of the anatase phase (C_A) in a rutile-anatase mixture can be calculated using the following formula (eqn. (2)) [9], [10]:

$$CA = \frac{8IA}{(8IA+13\ IR)} \qquad (2)$$

where IA and IR are x-ray peak intensities of anatase (101) and rutile (110) phases, respectively. Also, anatase and rutile phase crystallite size was calculated from XRD data using the Scherrer equation. A non-contact 3D optical profilometer (Alicona InfinteFocus SL) was used to characterise the surface roughness profile of the deposited specimens using a 5x objective. The analysed area was 25mm × 25mm for each coating. A tape adhesion test based on ASTM D3359-17 [11] was performed by cutting a 5×5 (at least) grid pattern of 1×1 mm squares into the sample surface using an Elcometer 1540 Cross Hatch Cutter to ensure that the scraped channels went through the coating and into the steel substrate beneath. Once the pattern was cut, Elcometer 99 Adhesion Test tape was carefully adhered to the surface. It was then pulled off at 180° to the sample surface in a single motion, and samples were examined for material loss and delamination.

3. Results and discussion

The average weight gain of all samples is presented in Figure 1 (a). It can be seen from the figure that the weight increases along with the increased feedstock flowrate, which can be explained as when more feedstock material is inserted into the plasma flame, after fragmentation, bigger droplets are formed that travel in the core region of the plasma and do not deviate from the path [12]. Hence, more material is deposited on the substrate, meaning more weight gain. In the case of SOD, the weight gain fluctuates with the feedstock flow rate. At a low feedstock flow rate (10 ml/min), the weight gain decreases with the increased SOD. This could be because, at a lower feedstock flow rate, smaller droplets with less material are formed, which, after evaporation of water, give rise to small-size agglomerates. Small droplets/particles tend to follow the gas trajectory and deviate from the central region, leading to less material deposition [12]. Simultaneously, coatings deposited at higher SOD (100mm) with a higher flow rate (30 ml/min) show more weight gain due to the formation of larger droplets hitting the substrate.

The deposition efficiency (DE) of all samples is shown in Figure 1 (b), and it was found that all samples show low DE. When spraying suspension feedstock, the solvent evaporates, and only solid content reaches the substrate. It should be noted that DE is the underestimated value due to the loss of feeding material during acceleration and deceleration and overspray of the torch robot [7]. Although a larger substrate can help resolve overspray to some extent (for smaller substrate, due to being carried away with the air flow, sprayed particles tend to overshoot the edges and lost to the surrounding environment. While in the case of larger substrate, a greatest distance is travelled by sprayed particles before reaching the edges, retaining more material on the substrate), the loss of feedstock material during acceleration and deceleration is unavoidable. The comparison of DEs is still valid as these accuracies are standard for each sample. Low DE is also associated with the radial injection of the feedstock material because, sometimes, the small droplets cannot reach the core region of the plasma plume. Instead, they deflect from their path, leading to insufficient energy exchange, and hence, poor deposition occurs. It was observed that at a lower flow rate (10 ml/min), with the increased SOD, DE decreases. This can be elucidated by the fact that when a smaller amount of material is introduced into the plasma after fragmentation, it leads to the formation of smaller droplets. These smaller droplets may not efficiently reach the substrate as they tend to follow the gas trajectory. So, more material is deposited at a smaller SOD (50mm), where the substrate is comparatively closer to the gun, and the kinetic energy is higher than at longer SODs (100mm). While DE increases for a higher feedstock flow rate (30 ml/min) at longer SODs because, due to the injection of more feedstock material, larger droplets are formed that have more inertia and higher kinetic energy compared to the smaller droplets. Hence, more material is deposited.

Preprints (www.preprints.org) | NOT PEER-REVIEWED | Posted: 25 October 2023 doi:10.20944/preprints202310.1545.v1

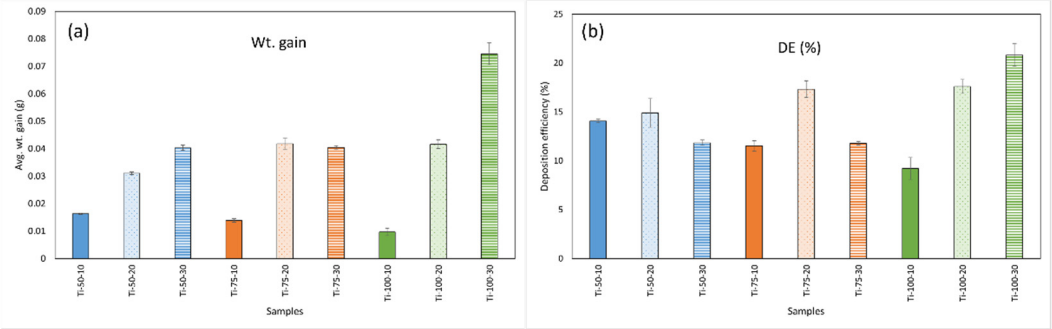

Figure 1. Average weight gain and deposition efficiency of different TiO_2 coatings.

The SEM images of TiO_2 coatings at different magnifications are shown in and Figure 3. All coatings show typical cauliflower-like topography due to the deposition of feedstock material in the asperities of the substrate after hitting it at shallow angles. This phenomenon is referred to as the "shadow effect," and it becomes more pronounced when dealing with smaller droplets. These smaller droplets deviate from their intended path as they follow the gas trajectory, often depositing on substrate asperities while moving parallel to the substrate surface [12].

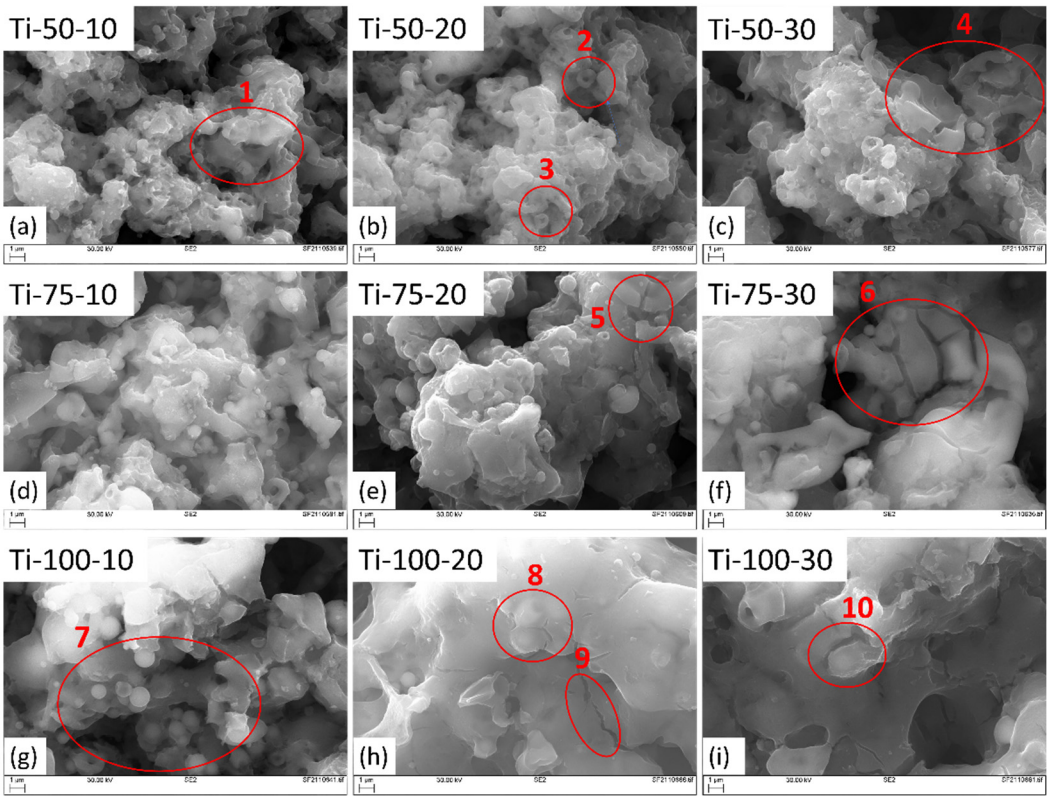

Figure 2. SEM images of different TiO_2 coatings at 1kX magnification.

It was found that fully-melted and thinner splats are formed at smaller SODs (; circle 1), while thicker splats with partially melted or re-solidified feedstock droplets (; circle 7) take place at longer SODs. This happens because, at smaller SOD, the thermal and kinetic energy of formed droplets are higher than the longer SODs. Hence, fully-melted droplets hit the substrate with a higher impact, spreading and covering the substrate properly. While at longer SODs, due to the insufficient thermal and kinetic energy transfer, rougher and thicker splats are formed. Also, at longer distances, nanomaterials, because of their high surface area, cool down very quickly and re-solidify even before

Preprints (www.preprints.org) | NOT PEER-REVIEWED | Posted: 25 October 2023 doi:10.20944/preprints202310.1545.v1

hitting the substrate or sticking to the surface, giving rise to voids after being trapped between subsequent splats [13].

With the increased feedstock flow rate, rougher splats formation, partial melting of feedstock droplets (; circles 2, 3, 8 & 9), and mud-like cracks formation (; 4, 5 & 6) also increase due to solvent evaporation. This can be explained by noting that when additional feedstock material is introduced, a greater volume of solvent (water) is also injected into the system. This additional solvent serves to cool down the flame. This leads to a comparatively lower heat transfer from the plasma to feedstock droplets. Hence, rougher and thicker splats and partial or no melting of TiO_2 droplets take place [14]. When these partially molten or unmolten particles deposit on the substrate, there is a difference in their temperature, microstructures, mechanical properties and bonding characteristics, and the non-uniform distribution of these particles, could result in localized stress concentrations, potentially generating mud-crack formation in certain parts of the coating..

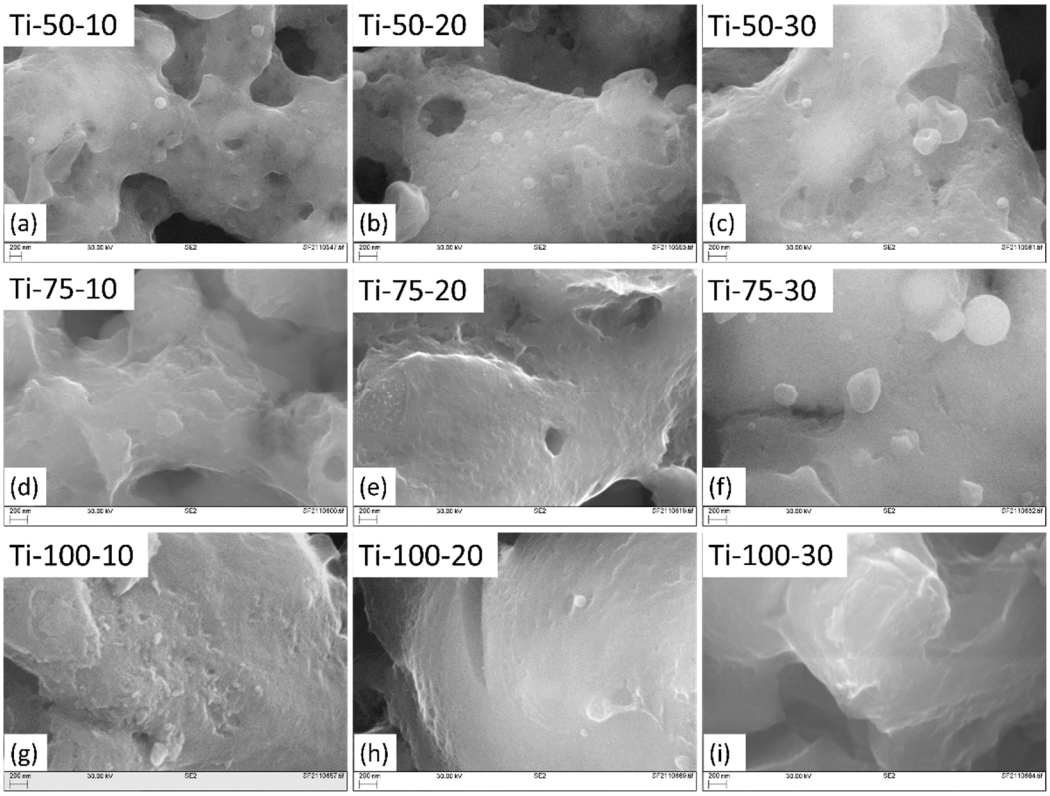

Figure 3. SEM images of different TiO_2 coatings at high magnification (10kX).

Cross-sectional back-scattered SEM images of developed coatings are shown in Figure 4. Since the substrate was pretreated with alumina grit blasting before coating deposition for better adhesion between coating and substrate, the formation of columnar structures is more favourable than vertical cracks or smooth coatings [15]. This happens because when particle droplets travel toward the substrate perpendicularly, only big particles possessing a high moment of inertia hit the substrate perpendicularly. Smaller particles easily get influenced by the drag force of the plasma trajectory and deviate from their original direction, impacting the substrate at a shallow angle, and deposit on the nearest asperities, forming columnar features (shadowing effect). After subsequent deposition and vertical and horizontal growth, cone-shaped structures are developed, where inter-columnar voids separate these cones/columns, and the head of columns gives rise to a typical cauliflower-like morphology [16].

Coatings deposited using 10ml/min do not exhibit column formation prominently due to the inefficient coverage of the substrate (thinner coatings). Simultaneously, coatings deposited at 50mm SOD show sharper peaks in cross-sections because of the high impact and kinetic energy of the particles, which hit the substrate with high accelerated force, depositing well-spread splat over the

Preprints (www.preprints.org) | NOT PEER-REVIEWED | Posted: 25 October 2023 doi:10.20944/preprints202310.1545.v1

substrate's asperities. As the coating gets thicker, column formation and their separation (inter-columnar voids) can be observed clearly (Figure 4 (e & f)) [16]. At longer SOD, due to inefficient kinetic and thermal energy exchange, thicker splats are formed that give rise to wide and comparatively round-shaped peaks. Also, it was found that with the increased feedstock flow rate, partially melted, un-melted, and agglomerated/sintered feedstock particles were observed more prominently, leading to more porous coating with vertical cracks formation (Figure 4 (c)). The coatings at 50 mm SOD, especially deposited using 20 and 30 ml/min feedstock flow rate, exhibited the presence of more partially melted or un-melted feedstock particles and more porosity as compared to the coatings developed at 75 mm SOD and 20 and 30 ml/min feedstock flow rate (Figure 4 e&f). This can be explained as, at a shorter distance, feedstock droplets do not get sufficient time for solvent evaporation, agglomeration, sintering, and melting, consequently giving rise to more porous coatings [17]. While at longer SOD, sometimes, melted material cools down even before hitting the substrate and, rather than forming a splat, adheres to the previously deposited splats.

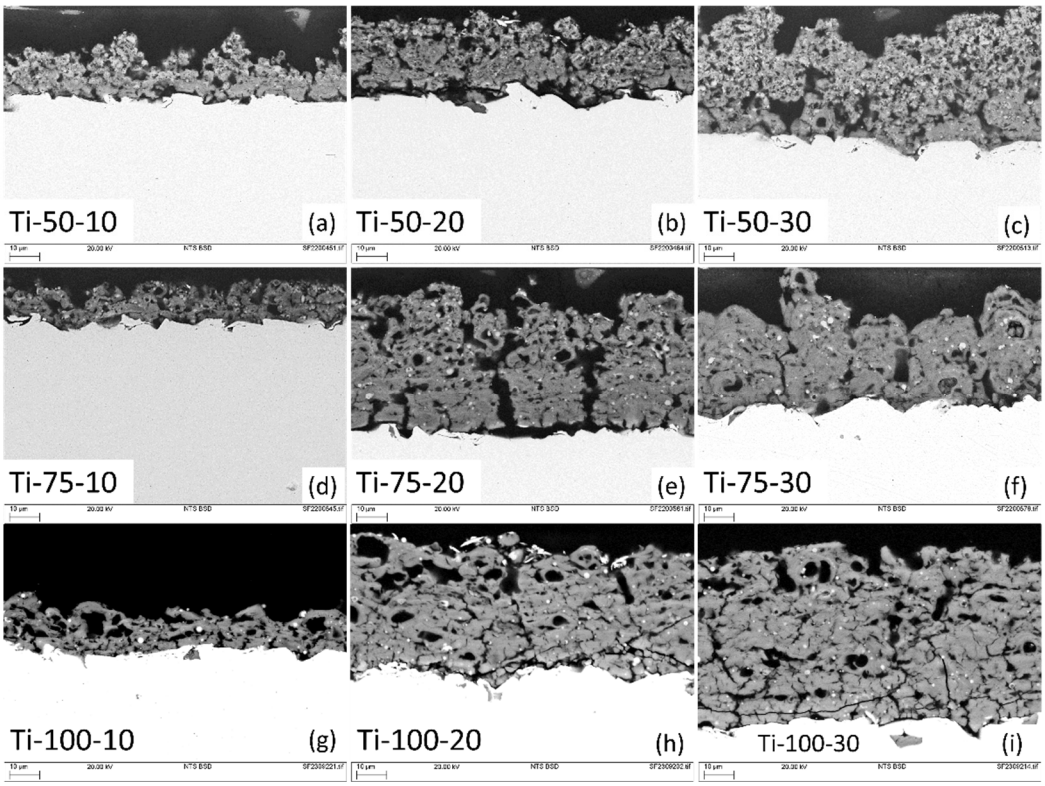

Figure 4. Cross-sectional back-scattered SEM images of different TiO_2 coatings.

The spray parameters are critical in influencing the particle impact energy, coating microstructures, and coating roughness. The R_a (average roughness), R_q (root mean square roughness), R_z (maximum height roughness), R_{ku} (kurtosis: sharpness of the surface's peaks and valleys), and R_{sk} (skewness: asymmetry of the surface) values are shown in Figure 5. It was found that with increased feedstock flow rate, the R_a, R_q, R_z, and R_{sk} increase because at a higher feedstock flow rate, particle accumulation, over-deposition, and insufficient particle flattening take place, resulting in a coating with higher porosity and rougher surface texture. With the feedstock flow rate, R_{ku} was increased but only for 50 mm SOD. In comparison, for 75mm and 100mm SODs, R_{ku} was almost similar, which means at 50mm SOD, due to the comparatively high impact of particles, sharper peaks and valleys are formed on the substrate's asperities. For Ti-50-20, the R_{sk} value was negative, indicating that there are more valleys or depressions on the surface than peaks.

The roughness values were almost similar for the coatings deposited at different SODs using a low feedstock flow rate, i.e., 10 ml/min. In comparison, this trend changes at higher 20 and 30 ml/min, resulting in a decreased roughness with the increased SOD. This can be elucidated by the fact that, at lower feedstock flow rates, the formation of flattened splats with extensive substrate coverage occurs.

Preprints (www.preprints.org) | NOT PEER-REVIEWED | Posted: 25 October 2023 doi:10.20944/preprints202310.1545.v1

This results in a well-adhered coating due to the adequate melting of the coating material. Also, it can be concluded that at higher SODs, the sharpness of peaks/columns decreases because the insufficient kinetic and thermal energy exchange gives rise to thicker (disc-like) splats, forming columns with globular heads after subsequent deposition [18,19].

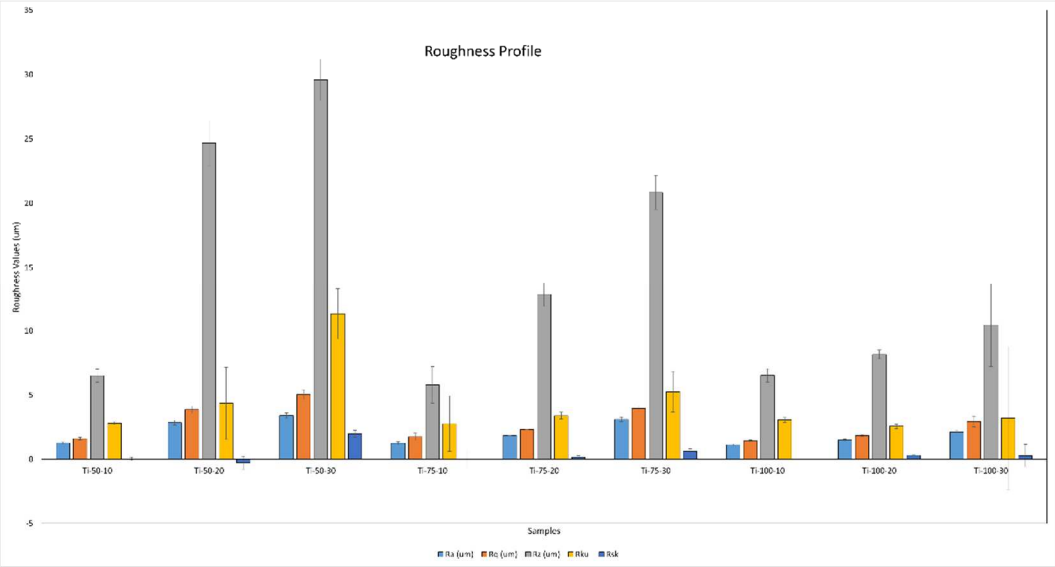

Figure 5. Roughness profile of different TiO_2 coatings.

The crystalline structure of TiO_2 coatings deposited at different spray conditions was analysed by comparing XRD data, shown in Figure 6. All coatings were found to show two main phases of TiO_2, i.e., anatase and rutile, and characteristic peaks related to the substrate. The peak intensity was highest for the coatings developed using a low feedstock flow rate because of low coating thickness. As the feedstock flow rate increases, the peak intensity of the substrate's characteristic peaks decreases. Various spray parameters, including SOD and feedstock flow rate, affect the phase formation and crystallite size of SPS coatings [18]–[20]. The crystallite size of coatings was calculated using the Scherrer equation to anatase (101) and rutile (110) peaks (Table 2). Regarding the anatase crystallite size, a reduction was noted with higher feedstock flow rates and a decrease in stand-off distance (SOD). This can be clarified by understanding that at longer spray distances, there is more time in-flight before reaching the substrate. This extended travel favours the formation of larger agglomerates, allowing for sufficient sintering of the material and leading to an increase in crystallite size [20]. At a higher feedstock flow rate, insufficient sintering or re-solidification due to the insertion of more solvent and reduced flame enthalpy leads to reduced crystallite size. For the rutile phase, it was observed that coatings deposited using 20ml/min exhibited larger crystallites. The possible explanation behind this could be that at 20ml/min, more solid content is present in the droplets, which, after efficient melting, agglomeration, and sintering, form larger crystallites as compared to the coatings deposited using 30ml/min, where comparatively insufficient melting occurs. Although no significant difference was observed in the anatase content of all deposited coatings, a slight increase was found in the anatase content with the increased SOD (Table 2). With the increased SOD, agglomerates have more time to re-solidify during flight, forming anatase phase proportions due to homogeneous nucleation. At the same time, agglomerates that solidify on the substrate (in the case of shorter SODs) can form anatase or rutile, depending on various factors, including agglomerate size. Usually, for agglomerates solidifying on the substrate, rutile phase formation is favoured due to the lower Gibbs free energy. However, if the agglomerate size is in the submicron range, metastable anatase phase formation takes place due to the fast solidification, suppressing the heterogeneous nucleation[20–22].

Preprints (www.preprints.org) | NOT PEER-REVIEWED | Posted: 25 October 2023 doi:10.20944/preprints202310.1545.v1

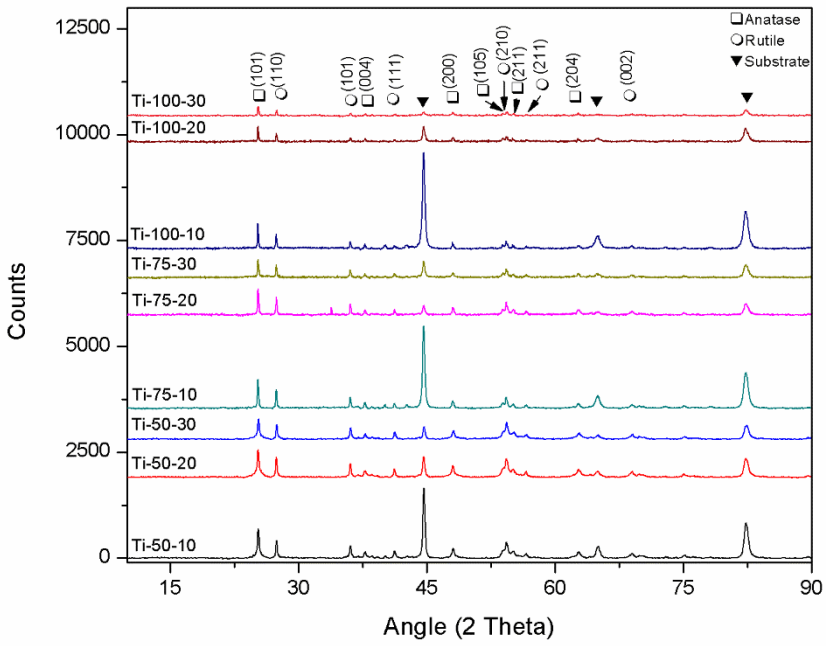

Figure 6. Comparison of XRD pattern of different TiO_2 coatings developed at varied SOD and feedstock flow rate.

Table 2. Comparison of volume percentage of anatase phase and anatase and rutile phase crystallite size of different TiO_2 coatings developed at varied SOD and feedstock flow rate.

Sample	Anatase content (C_A); %	Crystallite size (nm)	
		Anatase	Rutile
Ti-50-10	48	24.15	31.94
Ti-50-20	41	17.2	36.57
Ti-50-30	42	18.03	29.25
Ti-75-10	47	44.99	45.29
Ti-75-20	45	37.62	91.33
Ti-75-30	44	33.96	48.19
Ti-100-10	50	67.06	52.83
Ti-100-20	45	50.99	136.95
Ti-100-30	43	36.86	71.28

The macrographs of different coatings after performing tape adhesion tests (shown in Figure 7) show that the coatings deposited at a lower SOD, i.e., 50mm, were well adhered to the substrate due to high impact and comparatively better thermal energy transfer at low SOD between torch and feedstock particles. Also, coatings deposited using a low feedstock flow rate, i.e., 10 ml/min, showed good adhesion. When higher feedstock flow rates are used, along with more material, more solvent (water) is introduced, hence improper melting of particles due to cooling down of the plasma flame [7]. Therefore, Ti-75-20, Ti-75-30, Ti-100-20, and Ti-100-30 showed a high degree of delamination compared to others.

 doi:10.20944/preprints202310.1545.v1

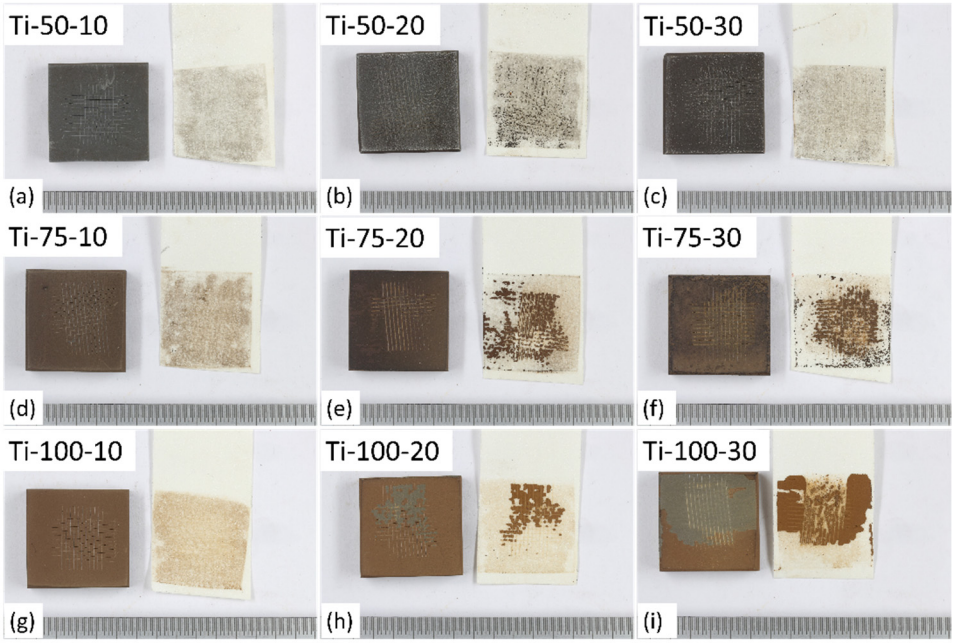

Figure 7. Macrographs of different TiO_2 coatings after tape adhesion test.

5. Summary and Conclusions

Coatings with superior performance help extend the lifetime of geothermal heat exchangers and improve the overall efficiency of geothermal power plants. Thermal spray TiO_2 coating could be an option to protect the components of geothermal heat exchangers from corrosion and scaling. In this study, TiO_2 coatings were deposited through suspension plasma spray using a uniform aqueous suspension of 5wt.% TiO_2 nanoparticles on carbon steel (S275JR, EN 10025-2) substrates, and to understand the role of different spray parameters in coating microstructures formation, the coatings were deposited at different standoff distances using different feedstock flow rates. It was found that at a small SOD, due to the proximity with the plasma torch, coating particles possess high thermal and kinetic energy, which leads to well-melted and smooth splat formation, hence, compact coatings. However, as the feedstock flow rate increased at a small SOD, poor melting of particles due to cooling of plasma plume, excessive material insertion, and insufficient time took place, and hence, porous coatings were formed. At larger SODs, due to the poor thermal and kinetic energy exchange between the torch and feedstock particles, resolidification of feedstock particles occurred and gave rise to porous coatings. The tape adhesion tests showed that coatings deposited at 50mm SOD (Ti-50-10, Ti-50-20 and Ti-50-30) and coatings deposited using 10ml/min feedstock flow rate (Ti-75-10 and Ti-100-10) were well adhered to the substrate in comparison to the coatings deposited using higher feedstock flow rate and at longer SODs (Ti-75-20, Ti-75-30, Ti-100-20, and Ti-100-30). The outcomes of this work offer a platform for further optimization and development of protective coatings for geothermal heat exchangers.

Author Contributions: Conceptualization, S.P.; methodology, S.P. and G.M.; investigation, G.M. and N.G.M.; formal analysis, G.M.; writing—original draft preparation, G.M. and A.B.N.J.; writing—review and editing, S.P.; supervision, S.P. and D.M.; Project administration, D.M. and N.K. All authors have read and agreed to the published version of the manuscript.

Funding: This project has received funding from the European Union's Horizon 2020 research and innovation programme under the project: GeoHex-advanced material for cost-efficient and enhanced heat exchange performance for geothermal application (Grant agreement 851917).

Acknowledgments: We want to acknowledge the contribution of the GeoHex consortium to this project.

Conflicts of Interest: The authors declare no conflict of interest.

References

1. [1] J. Nogara and S. J. Zarrouk, "Corrosion in geothermal environment: Part 1: Fluids and their impact," *Renewable and Sustainable Energy Reviews*, vol. 82, pp. 1333–1346, Feb. 2018, doi: 10.1016/j.rser.2017.06.098.
2. [2] D. E. Kim, D. I. Yu, D. W. Jerng, M. H. Kim, and H. S. Ahn, "Review of boiling heat transfer enhancement on micro/nanostructured surfaces," *Experimental Thermal and Fluid Science*, vol. 66, pp. 173–196, Sep. 2015, doi: 10.1016/j.expthermflusci.2015.03.023.
3. [3] P. Fauchais, M. Vardelle, A. Vardelle, and S. Goutier, "What Do We Know, What are the Current Limitations of Suspension Plasma Spraying?," *J Therm Spray Tech*, vol. 24, no. 7, pp. 1120–1129, Oct. 2015, doi: 10.1007/s11666-015-0286-3.
4. [4] D. Tejero-Martin, M. Rezvani Rad, A. McDonald, and T. Hussain, "Beyond Traditional Coatings: A Review on Thermal-Sprayed Functional and Smart Coatings," *J Therm Spray Tech*, vol. 28, no. 4, pp. 598–644, Apr. 2019, doi: 10.1007/s11666-019-00857-1.
5. [5] X. Chen, S. Kuroda, T. Ohnuki, H. Araki, M. Watanabe, and Y. Sakka, "Effects of Processing Parameters on the Deposition of Yttria Partially Stabilized Zirconia Coating During Suspension Plasma Spray," *Journal of the American Ceramic Society*, vol. 99, no. 11, pp. 3546–3555, 2016, doi: 10.1111/jace.14393.
6. [6] X. Zhang, Y. Wang, D. Zhao, and J. Guo, "Improved thermal performance of heat exchanger with TiO2 nanoparticles coated on the surfaces," *Applied Thermal Engineering*, vol. 112, pp. 1153–1162, Feb. 2017, doi: 10.1016/j.applthermaleng.2016.10.148.
7. [7] G. Mittal and S. Paul, "Suspension and Solution Precursor Plasma and HVOF Spray: A Review," *J Therm Spray Tech*, vol. 31, no. 5, pp. 1443–1475, Jun. 2022, doi: 10.1007/s11666-022-01360-w.
8. [8] 14:00-17:00, "ISO 17836:2017," ISO. Accessed: Aug. 30, 2023. [Online]. Available: https://www.iso.org/standard/69754.html
9. [9] N. Berger-Keller, G. Bertrand, C. Filiatre, C. Meunier, and C. Coddet, "Microstructure of plasma-sprayed titania coatings deposited from spray-dried powder," *Surface and Coatings Technology*, vol. 168, no. 2, pp. 281–290, May 2003, doi: 10.1016/S0257-8972(03)00223-8.
10. [10] F.-L. Toma, D. Sokolov, G. Bertrand, D. Klein, C. Coddet, and C. Meunier, "Comparison of the photocatalytic behavior of TiO2 coatings elaborated by different thermal spraying processes," *J Therm Spray Tech*, vol. 15, no. 4, pp. 576–581, Dec. 2006, doi: 10.1361/105996306X147225.
11. [11] "Standard Test Methods for Rating Adhesion by Tape Test." Accessed: Aug. 30, 2023. [Online]. Available: https://www.astm.org/d3359-17.html
12. [12] G. Mauer and R. Vaßen, "Coatings with Columnar Microstructures for Thermal Barrier Applications," *Advanced Engineering Materials*, vol. 22, no. 6, p. 1900988, 2020, doi: 10.1002/adem.201900988.
13. [13] L. Du, T. W. Coyle, K. Chien, L. Pershin, T. Li, and M. Golozar, "Titanium Dioxide Coating Prepared by Use of a Suspension-Solution Plasma-Spray Process," *J Therm Spray Tech*, vol. 24, no. 6, pp. 915–924, Aug. 2015, doi: 10.1007/s11666-015-0251-1.
14. [14] R. Rampon, O. Marchand, C. Filiatre, and G. Bertrand, "Influence of suspension characteristics on coatings microstructure obtained by suspension plasma spraying," *Surface and Coatings Technology*, vol. 202, no. 18, pp. 4337–4342, Jun. 2008, doi: 10.1016/j.surfcoat.2008.04.006.
15. [15] F. Caio and C. Moreau, "Influence of Substrate Shape and Roughness on Coating Microstructure in Suspension Plasma Spray," *Coatings*, vol. 9, no. 11, Art. no. 11, Nov. 2019, doi: 10.3390/coatings9110746.
16. [16] B. Bernard, L. Bianchi, A. Malié, A. Joulia, and B. Rémy, "Columnar suspension plasma sprayed coating microstructural control for thermal barrier coating application," *Journal of the European Ceramic Society*, vol. 36, no. 4, pp. 1081–1089, Mar. 2016, doi: 10.1016/j.jeurceramsoc.2015.11.018.
17. [17] A. Joulia, W. Duarte, S. Goutier, M. Vardelle, A. Vardelle, and S. Rossignol, "Tailoring the Spray Conditions for Suspension Plasma Spraying," *J Therm Spray Tech*, vol. 24, no. 1, pp. 24–29, Jan. 2015, doi: 10.1007/s11666-014-0184-0.
18. [18] P. Sokołowski, S. Kozerski, L. Pawłowski, and A. Ambroziak, "The key process parameters influencing formation of columnar microstructure in suspension plasma sprayed zirconia coatings," *Surface and Coatings Technology*, vol. 260, pp. 97–106, Dec. 2014, doi: 10.1016/j.surfcoat.2014.08.078.
19. [19] P. Sokołowski, L. Pawłowski, D. Dietrich, T. Lampke, and D. Jech, "Advanced Microscopic Study of Suspension Plasma-Sprayed Zirconia Coatings with Different Microstructures," *J Therm Spray Tech*, vol. 25, no. 1, pp. 94–104, Jan. 2016, doi: 10.1007/s11666-015-0310-7.

20. [20] B. W. Robinson *et al.*, "Suspension plasma sprayed coatings using dilute hydrothermally produced titania feedstocks for photocatalytic applications," *J. Mater. Chem. A*, vol. 3, no. 24, pp. 12680–12689, Jun. 2015, doi: 10.1039/C4TA05397D.
21. [21] E. Alebrahim, F. Tarasi, Md. S. Rahaman, A. Dolatabadi, and C. Moreau, "Fabrication of titanium dioxide filtration membrane using suspension plasma spray process," *Surface and Coatings Technology*, vol. 378, p. 124927, Nov. 2019, doi: 10.1016/j.surfcoat.2019.124927.
22. [22] E. Bemporad *et al.*, "Structural characterisation of High Velocity Suspension Flame Sprayed (HVSFS) TiO2 coatings," *Surface and Coatings Technology*, vol. 204, no. 23, pp. 3902–3910, Aug. 2010, doi: 10.1016/j.surfcoat.2010.05.011.